scientific reports

Check for updates

OPEN

Aluminum-derived nanotubes for lung cancer detection: a DFT inquisition

Aoly Ur Rahman[1,2,6]✉, D. M. Saaduzzaman[3,6], Syed Mahedi Hasan[4,6], Muzzakkir Amin[5,6] & Md. Kabir Uddin Sikder[6]

Lung cancer is one of the most pernicious health concerns and leading cause of mortality which is attributed to about two million deaths and four million new cases reported annually all over the world. So, a facile, quick, and non-invasive method of early detection of lung cancer is very crucial. Owing to the success of gas-sensing technology, this work proposed a novel work of developing sensors to diagnose lung cancer by analyzing the adsorption mechanism of three common volatile organic compound biomarkers- acetaldehyde, aniline, and isoprene on two Aluminum-derived nanotubes- Aluminum nitride (AlN) and Aluminum phosphide (AlP) via quantum mechanical approach DFT method. The adsorption energy confirms all the biomarkers will successfully adsorb on the AlNNT and AlPNT with an exothermic chemical reaction as well as AlNNT exhibits 26.30 ~ 29.66% more adsorption intensity than AlPNT for the corresponding biomarker. The absence of imaginary frequency in the IR spectrum for pristine and complex nanotubes confirms that the geometries belong to true energy minima and tend to form naturally. Also, the analyses of different electrical and thermodynamical properties strongly support the favor of AlNNT as sensory material. Based on the light of all factors, AlNNT could be a potential candidate for developing biosensors to diagnose lung cancer in its early stages.

Keywords Lung cancer, DFT, Group III-V nanotubes, Early detection of cancer, Biosensor

Lung cancer is responsible for the leading cause of cancer concerning mortality which is attributed to about two million deaths and four million new cases are reported annually all over the world[1–4]. The effective factors of the mortality of lung cancer have a wide range of variety such as age, sex, geographic changes, ethnicity, socioeconomic condition, and so on that lead to an alarming prediction of the death of lung cancer patients about 3.2 million by 2050 [2,5]. However, a lot of clinical studies confirm that early detection and treatment of lung cancer help to reduce the mortality rate[6]. At present, the detection of lung cancer has been done using some popular diagnostic techniques such as chest radiographs, computed tomography scans (CT scan), magnetic resonance imaging technique (MRI), positron emission tomography (PET), and cytology sputum, biopsy, breath analysis and so on[7–10]. However, these current diagnostic techniques are associated with crucial challenges such as high costs, invasiveness, false reports, and so on, making the situation more critical[11–14]. So, developing rapid, simple, non-invasive early diagnosis techniques for detecting cancer has become a great concern for researchers[15,16]. In recent years, due to the development of nanoscience and technology, different low-dimensional materials such as nanosheets, nanotubes, nanodots, etc. have been extensively used in various technological, especially in biomedical and sensing applications[17–21]. In 2019, Roberts et al. developed a Fluorine-doped tin oxide-based graphene nanosheet as an immunosensor for rapidly detecting urokinase-type plasminogen activator receptor, a well-known cancer biomarker. From their experiment, they observed that the developed immunosensor showed better reproducibility, repeatability, and storage stability which is 75% more than the initial activity[19]. In 2024 Sakr et al. investigated the adsorption properties of biphenylene quantum dot along with its metal oxide (CuO, ZnO, TiO_2, and V_2O_5) before and after adsorbing glucose which is primarily considered a biomarker of diabetes using density functional theory (DFT) and found that all the structures are stable and the reaction process is spontaneous[20]. However, among miscellaneous nanomaterials, nanotubes exhibit greater sensitivity toward

[1]Department of Nanomaterials and Ceramic Engineering, Bangladesh University of Engineering & Technology, Dhaka, Bangladesh. [2]Department of Physics, Dhaka University of Engineering & Technology, Gazipur, Bangladesh. [3]Department of Materials Science and Engineering, Rensselaer Polytechnic Institute, Troy, New York, USA. [4]Department of Physics, Florida Institute of Technology, Melbourne, Florida, USA. [5]Department of Materials and Bio Materials Science and Engineering, University of California, Merced, USA. [6]Department of Physics, Jahangirnagar University, Savar, Dhaka, Bangladesh. ✉email: aolyurrahman@gmail.com

diverse biomolecules because of their unique physicochemical properties greater surface areas with preferable chemical stabilities as well as affluent electronic polyaromatic structure making them perfect fits for advancing sensing materials[22–26]. In 2022, Chen et al. developed functionalized carbon nanotube (CNT) based field-effect transistor (FET) to achieve higher sensitive and selective detection of blood biomarkers of β-amyloid to diagnose Alzheimer's disease and found that the aptamer-functionalized CNT-based FET biosensor exhibits a large dynamic range as well as rapid response time, and low variation which can be helpful to develop a low-cost and rapid clinical detection technology for the early diagnosis of Alzheimer's disease[25]. In the same year, using DFT theory Aasi et al. proposed the potentiality of platinum-decorated single-walled carbon nanotubes as a promising material for detecting octanol, decane, and hexanal as liver cancer biomarkers as the experimented biomarkers have strongly chemisorbed on the targeted nanotube along with preferable recovery time[26]. Therefore, consequencing the favorable outcome of different nanotubes, group III-IV nanotubes have drawn the attention of researchers in diverse sensing applications[27–29]. In 2023, using the DFT method, Kadhim et al. investigated the feasibility of antisite defect of Aluminum phosphide (AlP) nanotube for detecting ozone gas and observed that ozone shows weak interaction with the pristine and the phosphorus antisite AlPNT but in the case of Aluminum antisite the adsorption mechanism drastically improved for O_3 gas[27]. In the same year, Kadhim et al. investigated the selective adsorption behavior of toxic chloropicrin on Cd-doped Aluminum nitride nanotube (AlNNT) using the DFT approach and found that Cd-decoration enhances the adsorption energy of AlNNT from − 6.0 to − 22.4 kcal/mol for chloropicrin[28].

Owing to the successes of analytical chemistry and nano-sensing technologies, diagnosing different diseases by analyzing the breath of patients has become popular because of its non-invasiveness, rapidity, and cost-effectiveness[30–34]. In 2026, Sun et al. summarized the potentiality of diagnosis of different cancers from exile gas by detecting volatile organic compounds (VOCs) and tabulated the presence of different unique VOCs in the breath of nine different types of cancer patients (lung cancer, breast cancer, colon cancer, esophagogastric cancer, gastric cancer, head and neck cancer, liver cancer, ovarian cancer, and prostate cancer)[30]. In 2018 Wan et al. investigated the adsorption mechanism of two biomarkers of lung cancer that are benzene (C_6H_6) and aniline (C_6H_7N) on transition metal Rhodium (Rh) doped carbon nanotube (CNT) using the DFT approach and found the suitability of doped nanotube to detect those volatile organic compounds for early diagnosis of lung cancer[31]. Again in 2021, Tarun et al. using the DFT method investigated the adsorption behavior of three volatile organic compounds that are aniline, isoprene, and o-toluidine, on pristine and mono vacancy GaAs nanoribbons to understand the feasibility of GaAs nanoribbons as lung cancer sensory materials and found that the defect causes drastic improvement in sensing which leads them to conclude the potentiality of mono atom defected GaAs nanoribbons to sense aniline, isoprene and o-toluidine from the breath of lung cancer patients[34]. Further, in 2024 using the DFT method, Rahman et al. investigated the interactions of two biomarkers, 2-methyl octane (C_9H_{20}) and 3, 3-dimethyl pentane (C_7H_{16}) that present in the breath of breast cancer patients with Aluminum phosphide nanotubes (AlPNT) and gallium phosphide nanotubes (GaPNT) and concluded that in between these two nanotubes, GaPNT exhibits greater sensitivity toward C_9H_{20} and C_7H_{16} and could be used in developing sensing material for breast cancer detectors[29].

Based on all the discussed literature, we are motivated to conduct a DFT investigation on two aluminum-derived nanotubes, Aluminum nitride nanotube (AlNNT) and Aluminum phosphide nanotube (AlPNT) to analyze their ability to adsorb Acetaldehyde (C_2H_4O), Aniline (C_6H_7N), and Isoprene (C_5H_8), three common biomarkers present in the breath of lung cancer patients which are confirmed by distinct researches[30,31,34–36]. Therefore, the adsorption mechanism of C_2H_4O, C_6H_7N, and C_5H_8, on AlNNT and AlPNT concerning the structural, electric, thermodynamic, and optical changes of the studied Aluminum-derived nanotubes are investigated in detail to understand how these changes in physicochemical properties confirm the presence of these biomarkers and the viability of these nanotubes for developing sensory materials for early detection of lung cancer are also explored in this work. We anticipate that this computational study will help to develop sensors that can detect C_2H_4O, C_6H_7N, and C_5H_8 in order to diagnose lung cancer in the preliminary stage, and as far as we are concerned, no empirical or even theoretical study has been performed yet to detect C_2H_4O, C_6H_7N, and C_5H_8 with the help of AlNNT and AlPNT.

Computational description

In this work, to understand the adsorption behavior of studied nanotubes (AlNNT and AlPNT) and biomarkers present in the breath of lung cancer patients, all the nanotubes along with three targeted biomarkers Acetaldehyde (C_2H_4O), Aniline (C_6H_7N), and Isoprene (C_5H_8) have been designed in Gaussview 06 program[37] and optimized employing the quantum mechanical approach density functional theory (DFT)[38] along with LanL2DZ basis sets[39,40] and hybrid dispersion correlation functional B3LYP-D3 for non-covalent interactions[41,42] between adsorbent and adsorbate structures in the Gaussian 09 software package[43]. This combination of hybrid functional and basis set was used due to its associated accuracy observed in former studies[39–42]. Also, to optimize all the geometries successfully, 1000 cycles along with the quadratically convergence criteria for self-consistent field (SCF) equations (tolerance in the order of 10^{-5}) have been chosen, which is considered enough to relax structures with similar configurations[44,45]. In order to build the targeted adsorbents, at first instance, Aluminum nitride (AlN) and Aluminum phosphide (AlP) nanotubes ($Al_{10}N_{10}$ and $Al_{10}P_{10}$) having 20 atoms along with the tube length of 7 and 8Å respectively for AlNNT and AlPNT have been designed with armchair geometry (chirality 2, 2)[46] and because of nominating nonperiodic boundary conditions in the Gaussian 09 program, default K points have been used during the optimization process of achieving the nanotubes to the lowest ground state energy as well as the highest structural stability. In the same way, the adsorbed volatile organic compounds (VOCs) biomarkers C_2H_4O, C_6H_7N, and C_5H_8 have been designed and relaxed. Then these biomarkers were further adsorbed on AlNNT and AlPNT and formed six complexes those are AlNNT + C_2H_4O,

AlNNT + C_6H_7N, AlNNT + C_5H_8, AlPNT + C_2H_4O, AlPNT + C_6H_7N, and AlPNT + C_5H_8 and these complexes have been optimized in the same manner in the highest stable form to investigate physicochemical properties.

To understand the adsorption mechanism of the complex systems (nanotubes + VOCs), the adsorption energy has been computed using the following equation[47].

$$E_{AE} = E_{\text{Total (Nanotubes+VOCs)}} - (E_{\text{Nanotubes}} + E_{\text{VOCs}}) \quad (1)$$

Where E_{AE} is the adsorption energy while adsorbate VOCs (C_2H_4O, C_6H_7N, and C_5H_8) have been adsorbed in different adsorbent Nanotubes (AlNNT and AlPNT). Also, the basis set superposition error (BSSE) has been measured considering the counterpoise for computing the adsorption energy that is discussed in details in the corresponding section by using the following equation[48].

$$E_{AE_C} = E_{AE} + E_{BSSE} \quad (2)$$

The adsorbing distances between adsorbent nanotubes and the VOCs have been manually measured using the GaussView 6 software[37].

The recovery time of the complex system is another important factor in understanding the adsorption mechanism and helps to understand the required time period when the complex system releases the adsorbate VOCs and returns the former state is calculated by the following equation[49].

$$\tau = \frac{1}{\vartheta_0} e^{-\frac{E_{AE}}{K_B T}} \quad (3)$$

Where ϑ_0 is the initial applied UV frequency that is 10^{18} s^{-1}, K_B is the Boltzmann constant (8.62×10^{-5} eV K^{-1}) and T is the standard room temperature which values 298.16 K.

To investigate the electrical behavior of the complexes, different electrical properties such as the Mulliken charge, Natural bond orbital (NBO), Dipole moment, highest occupied molecular orbital (HOMO), lowest unoccupied molecular orbital (LUMO), HOMO-LUMO gap (ΔE), density of states (DOS) and Fermi energy level (E_F) have been measured before and after the adsorption has taken places employing the same level of theory in the Gaussian 09 program as described earlier.

The HOMO-LUMO gap (ΔE), and Fermi energy level (E_F) have been measured using the following equations[50,51].

$$\Delta E = E_{LUMO} - E_{HOMO} \quad (4)$$

$$E_F = \frac{E_{LUMO} + E_{HOMO}}{2} \quad (5)$$

To understand the optical behavior of the nanotubes before and after the adsorption process has taken place, different optical properties such as the molar adsorption coefficient (ε) as well as the circular dichroism (CD) spectrum to understand the optical chirality, in the presence of UV-visible response of the nanotubes, is observed in the TDDFT theory in Gaussian 09 program.

Also, the thermodynamic stability has been observed in computing different thermodynamic properties such as the changes in the Gibbs free energy, enthalpy, and entropy of the complex system after adsorbing the VOCs into different nanotubes have been measured in the standard room temperature T = 298.16 K in the Gaussian 09 program using the following equation[51].

$$\Delta G = G_{\text{Total (Nanotubes+VOCs)}} - (G_{\text{Nanotubes}} + G_{\text{VOCs}}) \quad (6)$$

$$\Delta H = H_{\text{Total (Nanotubes+VOCs)}} - (H_{\text{Nanotubes}} + H_{\text{VOCs}}) \quad (7)$$

$$\Delta S = \frac{\Delta H - \Delta G}{T} \quad (8)$$

Where ΔG is the changes in the Gibbs free energy, ΔH is the changes in enthalpy, and ΔS is the changes in the entropy of the complex systems after adsorbing the VOCs into different nanotubes at standard room temperature T = 298.16 K.

Result and discussion

Structural properties analyses

Equilibrium configurations

To understand different properties initially, armchair geometries of having chirality 2,2, Aluminum nitride (AlN) and Aluminum phosphide (AlP) nanotubes ($Al_{10}N_{10}$ and $Al_{10}P_{10}$) consisting of 20 atoms along with the tube length of 7Å and 8Å respectively for AlNNT and AlPNT have been designed and then relaxed to the lowest ground state energy in order to get the highest structural stability of the nanotubes. After obtaining the structures with the highest stability, the total ground state energies AlNNT and AlPNT have been found to be -15454.220 eV, and −2323.193 eV respectively as well as the diameters are 3.71 Å and 4.88 Å for AlNNT and AlPNT respectively. All the volatile organic compounds (VOCs) biomarkers have been relaxed in the same manner and obtained total ground state energies of -4185.334 eV, -7825.043 eV, and −5313.938 for C_2H_4O, C_6H_7N, and C_5H_8 respectively. After adsorbing these biomarkers on the targeted nanotubes, the obtained total

ground state energies for the highest stable complexes are −19642.082, −23282.419, −20770.559, −6510.476, −10150.72 eV, and −7639.032 for AlNNT + C_2H_4O, AlNNT + C_6H_7N, AlNNT + C_5H_8, AlPNT + C_2H_4O, AlPNT + C_6H_7N, and AlPNT + C_5H_8 respectively. The higher values of ground state energies for the adsorbed structures signify better structural stability of the adsorbed structures. The total ground state energies of all structures have been tabulated in (Table 1) and all the optimized geometries before and after the adsorption process has taken place have been illustrated in (Fig. 1).

Adsorption mechanism analyses

Adsorption energy is an important factor in understanding the adsorption behavior as well as the nature of the reaction between the adsorbent nanotubes and adsorbate the VOCs biomarkers. If the adsorption energy of the complex (after adsorbing the biomarkers) is negative, it signifies the exothermic as well as spontaneous nature of the reaction whereas the positive values of adsorption energy signify the endothermic and nonspontaneous nature of the reaction[29,48]. Furthermore, greater negative values in adsorption energy represent higher adsorption intensity and vice versa[52]. The computed adsorption energies of all the complex systems after adsorbing the biomarkers have been tabulated in (Table 1).

From the tabulated data, while acetaldehyde (C_2H_4O), aniline (C_6H_7N), and isoprene (C_5H_8) have been adsorbed on AlNNT the adsorption energy has been observed −2.527, −3.157, and −2.401 eV respectively and this adsorption energy has become −1.949, −2.484, and −1.901 eV respectively for AlPNT which clarifies that for the same biomarker, higher adsorption occurs in AlNNT than AlPNT. This means AlNNT exhibits more spontaneity along with a greater exothermic in nature while the adsorption process is taking place than AlPNT towards the adsorption of the same biomarker[48,52]. Also, in between AlNNT and AlPNT, AlNNT exhibits 29.66% more adsorption energy for C_2H_4O, 27.10% more for aniline, and 26.30% more for isoprene than AlPNT. This higher adsorption intensity confirms the betterment of AlNNT to detect acetaldehyde (C_2H_4O), aniline (C_6H_7N), and isoprene (C_5H_8) in order to develop sensors than AlPNT. For a better understanding, a graphical illustration has been depicted in Fig. 2 to show the comparative analyses of adsorption energies for targeted biomarkers.

The basis set superposition error (BSSE) has been also measured considering the counterpoise which is crucial in order to get accurate values of adsorption energies when the adsorbate molecules interact with adsorbent materials[48]. Therefore, considering the basis set superposition error, the corrected values have been obtained as −3.807, −4.719, and −3.247 eV respectively when C_2H_4O, C_6H_7N, and C_5H_8 biomarkers are adsorbed on AlNNT and −2.206, −2.946, −1.938 eV respectively for AlPNT. So, the former pattern of better adsorption behavior of AlNNT remains the same for the counterpoise correction.

Adsorbing distance is another significant parameter to understanding physisorption behavior while the adsorbent material adsorbs the adsorbate molecules and a smaller distance between adsorbent and adsorbate structures refers greater possibility of adsorbate-adsorbent interaction and vice versa[29,53]. To comprehend the adsorption intensity between the adsorbent nanotube and adsorbed biomarkers, the adsorbing distances between adsorbent nanotubes and targeted volatile organic compounds have been measured and tabulated in (Table 2). From the data, it has been observed that when C_2H_4O, C6H7N, and C_5H_8 are adsorbed on AlNNT, the measured distances between AlNNT and the corresponding VOC are 1.961, 2.051, and 2.503 Å respectively whereas in the case of AlPNT, the observed adsorbing distances are 3.248, 2.571, and 2.915 Å respectively for the same VOC. Therefore, between these two studied nanotubes, AlNNT shows 39.62% smaller adsorbing distance for C_2H_4O, 20.23% smaller for C6H7N, and 14.13% smaller for C_5H_8 than AlPNT which refers to an interesting key factor that this smaller adsorbing distance for AlNNT than AlPNT supports our former findings of greater adsorption energies as well as stronger physisorption nature of C_2H_4O, C6H7N, and C_5H_8 biomarkers on AlNNT and consequently this greater adsorption leads to a higher degree of recovery time during the desorption process[48]. In Fig. 3, comparative adsorbing distances have been illustrated for a better understanding.

Systems	E_{AE} (eV)	TGSE (eV)	MC (Q)	NBO (Q)	DM (Debye)	E_{HOMO} (eV)	E_{LUMO} (eV)	ΔE (eV)	E_{FL} (eV)
AlNNT	–	−15454.220	1.463	2.051	0.000	−5.901	−3.386	2.516	−4.643
AlPNT	–	−2323.193	0.625	1.137	0.000	−6.396	−4.252	2.144	−5.324
acetaldehyde (C_2H_4O)	–	−4185.334	0.643	0.723	3.279	−7.143	−1.191	5.952	−4.167
Aniline (C_6H_7N)	–	−7825.043	0.705	0.866	1.908	−5.334	−0.006	5.328	−2.670
Isoprene (C_5H_8)	–	−5313.938	0.754	0.664	0.754	−6.293	−0.869	5.424	−3.581
AlNNT + acetaldehyde	−2.527	−19642.082	1.524	2.062	5.612	−5.561	−3.041	2.521	−4.301
AlNNT + aniline	−3.157	−23282.419	1.468	2.076	7.803	−5.341	−2.786	2.555	−4.063
AlNNT + isoprene	−2.401	−20770.559	1.484	2.093	5.530	−5.473	−3.216	2.257	−4.344
AlPNT + acetaldehyde	−1.949	−6510.476	0.686	1.190	4.743	−6.179	−4.014	2.166	−5.097
AlPNT + aniline	−2.484	−10150.720	0.704	1.219	7.040	−5.979	−3.814	2.165	−4.897
AlPNT + isoprene	−1.901	−7639.032	0.773	1.187	1.575	−6.329	−4.195	2.134	−5.262

Table 1. The values of adsorption energies E_{AE} in eV, total ground state energy (TGSE) in eV, Mulliken charge (MC) in Q, natural bond orbital (NBO) in Q, dipole moment (DM) in Debye, HOMO energies (E_{HOMO}) in eV, LUMO energies (E_{LUMO}) in eV, HOMO-LUMO gaps (ΔE) in eV and Fermi energy level (E_{FL}) in eV of all the structures.

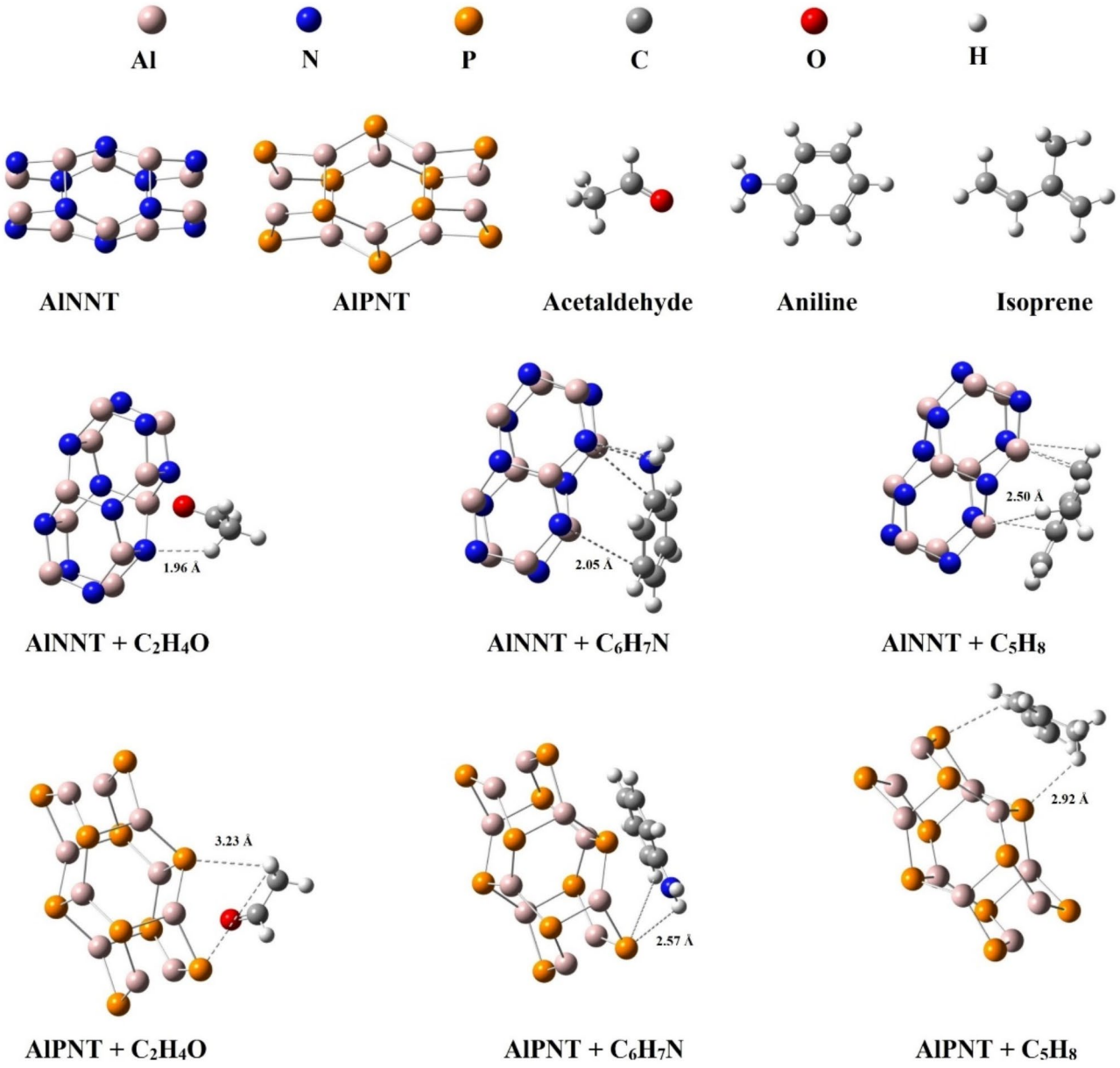

Fig. 1. Optimized structures of the AlNNT and AlPNT along with three VOCs C_2H_4O, C_6H_7N, and C_5H_8 before and after the adsorption process.

To understand the desorption mechanism of the complex system (adsorbent nanotubes + adsorbate VOCs), the recovery time is very crucial to study as it refers to the required time to release the adsorbed VOCs from the complex system and return the adsorbent nanotube to the former phase[49]. Moreover, the order of recovery time acts as proportional to the adsorption energy that is greater negative values in adsorption energy signify a stronger reaction as well as greater time to desorption[53]. To calculate the recovery time, the initial applied UV has been considered as 10^{18} s^{-1} with standard room temperature which values 298.16 K, and with the help of Eq. (3) all data for corresponding structures has been measured and tabulated in (Table 2).

From the tabulated data, it has been observed that the recovery times for AlNNT + C_2H_4O, AlNNT + C_6H_7N, AlNNT + C_5H_8 complexes are 5.02×10^{24}, 2.22×10^{35}, and 3.73×10^{22} s respectively and these values are 8.58×10^{14}, 9.42×10^{23}, 1.33×10^{14} s respectively for AlPNT + C_2H_4O, AlPNT + C_6H_7N, and AlPNT + C_5H_8 complexes. So, it is apprehensible that the higher recovery time indicates being suitable enough for analyzing the presence of VOCs from the complexes and also impractical of the conventional method of spontaneously regenerating the adsorbent through chemical reaction and in this regard the changing in initial applied frequency ϑ_0 as well as the temperature can be improved. To overcome this challenge of higher recovery time of adsorbed nanostructures, increasing system temperature is a popular method and distinct former studies suggested that applying high temperature (up to 1200 K) to make the desorption process quicker and get a reasonable recovery time[54,55]. Therefore using 600 K temperature, the obtained recovery times for AlNNT + C_2H_4O, AlNNT + C_6H_7N,

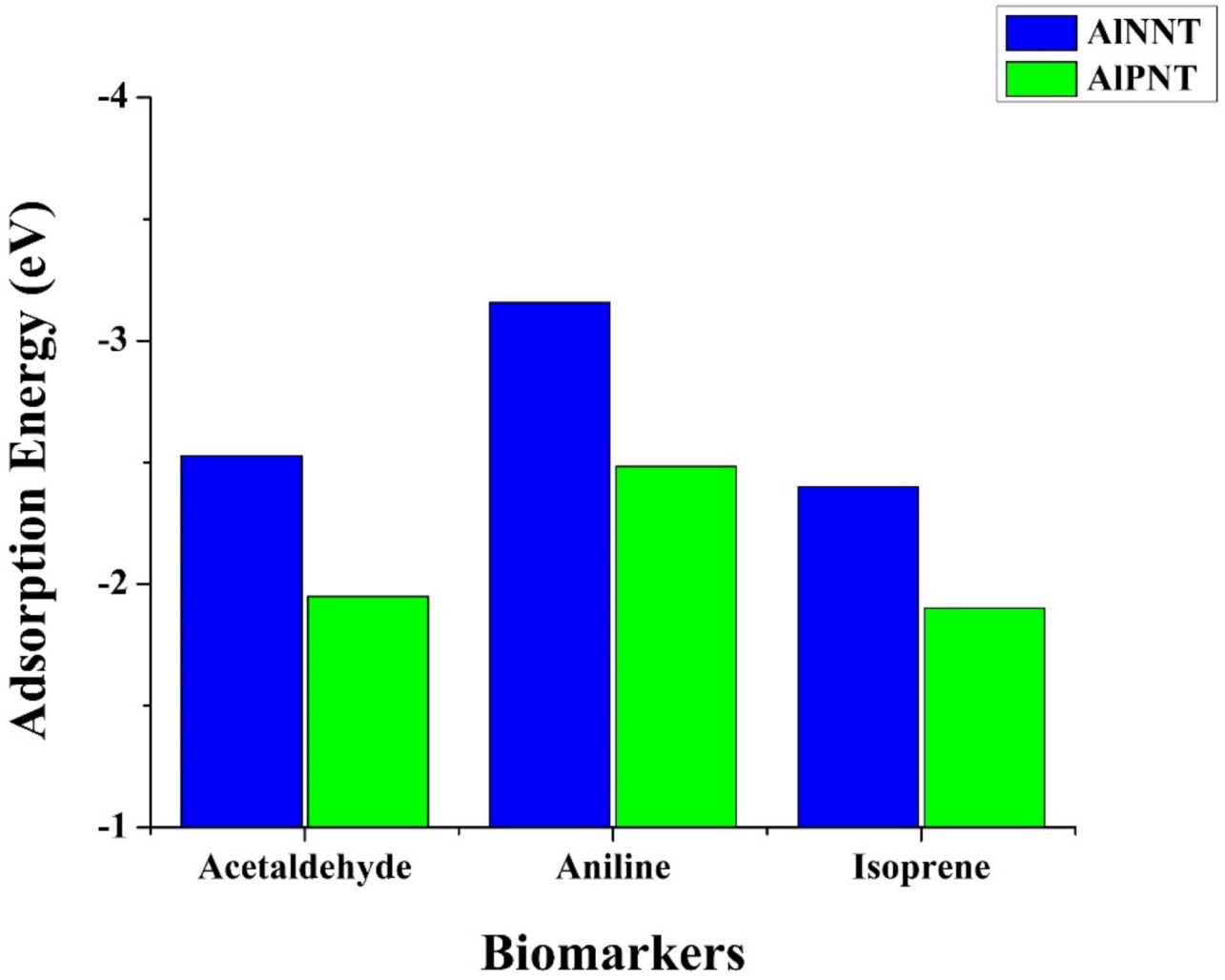

Fig. 2. Graphical presentation of the comparative adsorption energies of C_2H_4O, C_6H_7N, and C_5H_8 biomarkers for AlNNT and AlPNT.

Systems	D_{Ad} (Å)	τ (s)	ΔG (eV)	ΔH (eV)	ΔS (meV/Mol K)
AlNNT + acetaldehyde	1.961	5.02×10^{24}	−1.930	−2.458	−1.772
AlNNT + aniline	2.051	2.22×10^{35}	−2.494	−3.045	−1.848
AlNNT + isoprene	2.503	3.73×10^{22}	−1.800	−2.329	−1.776
AlPNT + acetaldehyde	3.248	8.58×10^{14}	−1.421	−1.912	−1.648
AlPNT + aniline	2.571	9.42×10^{23}	−1.860	−2.43	−1.913
AlPNT + isoprene	2.915	1.33×10^{14}	−1.366	−1.863	−1.666

Table 2. The tabulated values of adsorbing distances D_{AD} in Å, recovery time τ in second, changes in Gibbs free energy (ΔG) in eV, changes in enthalpy (ΔH) in eV, and changes in entropy (ΔS) in meV/Mol K.

AlNNT + C_5H_8 complexes have become 1.66×10^{3}, 3.23×10^{8}, and 1.45×10^{2} s respective and 2.32×10^{-2}, 7.21×10^{2}, and 9.18×10^{-3} s respectively for AlPNT + C_2H_4O, AlPNT + C_6H_7N, and AlPNT + C_5H_8 complexes. Also, the recovery time has obtained 1.40×10^{-4}, 4.71×10^{-1}, 2.76×10^{-5}, 8.14×10^{-8}, 8.04×10^{-5}, and 4.38×10^{-8} s respectively for AlNNT + C_2H_4O, AlNNT + C_6H_7N, AlNNT + C_5H_8, AlPNT + C_6H_7N, and AlPNT + C_5H_8 complexes when 900 K temperature is applied. Moreover, some regenerating agents such as HCl, NaOH, HNO_3, $NaHCO_3$, etc. can be applied to obtain better performance of making desorption process quicker[48,56].

IR spectrum analysis

The infrared (IR) spectrum provides the idea about the molecular vibration of the complex systems (adsorbent nanotube + adsorbate biomarkers) as well as their possibility to form naturally or not. The negative imaginary

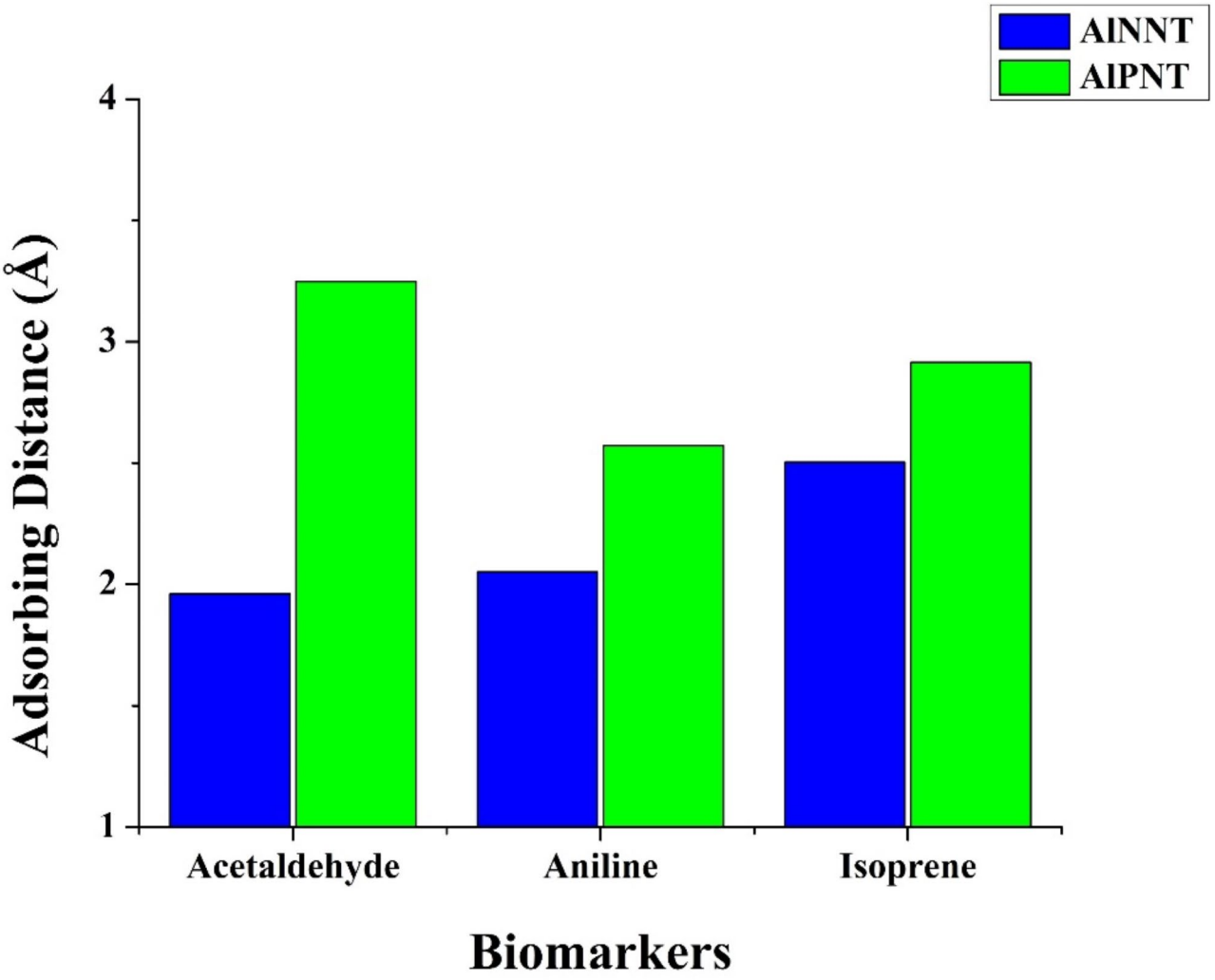

Fig. 3. Graphical representation of the comparative adsorbing distances while C_2H_4O, C_6H_7N, and C_5H_8 biomarkers have been adsorbed on AlNNT and AlPNT.

frequency in the IR spectrum predicts the inability of the complex to form naturally as well as the optimized geometry does not belong to true energy minima and vice versa[45,57]. The IR spectrum has been plotted to understand the molecular vibration of the nanotubes before and after adsorbing the studied biomarkers in (Fig. 4). For plotting the graphs, the frequency ranges have been selected from 0 to 4000 cm^{-1} as all the peaks are observed within these ranges. In the case of AlNNT, before the adsorption of VOCs has taken place two sharp peaks are observed near 600 and 1000 cm^{-1} but as the biomarkers are adsorbed on AlNNT, new lower amplitude peaks are observed between 1000 and 4000 cm^{-1}. This appearance of new secondary peaks refers to the stretching and bending of the complex systems due to the adsorption of targeted VOCs in AlNNT. A similar phenomenon is also observed for AlPNT while C_2H_4O, C_6H_7N, and C_5H_8 biomarkers have been adsorbed. Moreover, the absence of imaginary frequencies refers to all complexes that are AlNNT and AlPNT and formed six complexes those are AlNNT + C_2H_4O, AlNNT + C_6H_7N, AlNNT + C_5H_8, AlPNT + C_2H_4O, AlPNT + C_6H_7N, and AlPNT + C_5H_8 are likely to form naturally as well as the optimized complex geometries belong to true energy minima which supports the condition of highest structural stability[47,57].

Electrical properties analyses

Charge analyses

Mulliken charge distribution plays a significant role in comprehending the electrical property of any system, which refers to the natural population and partially shared charges among the sub-shells of molecular orbital[58]. Moreover, the Mulliken charge analyses help to develop sensory devices to detect any molecule by observing detectable electrochemical signals in the presence of that molecule[52]. All the measured Mulliken charges have been tabulated in (Table 1). From the tabulated data, it has been observed that the Mulliken charges of pristine AlNNT and AlPNT and three targeted biomarkers C_2H_4O, C_6H_7N, and C_5H_8 are 1.463, 0.625, 0.643, 0.705, and 0.754e respectively. In light of the Pauling scale, the electronegativity of the constituent atoms of nanotubes and biomarkers that are Al, N, P, C, H, and O are 1.5, 3.0, 2.1, 2.5, 3.5, and 2.2e respectively[59]. Therefore, after

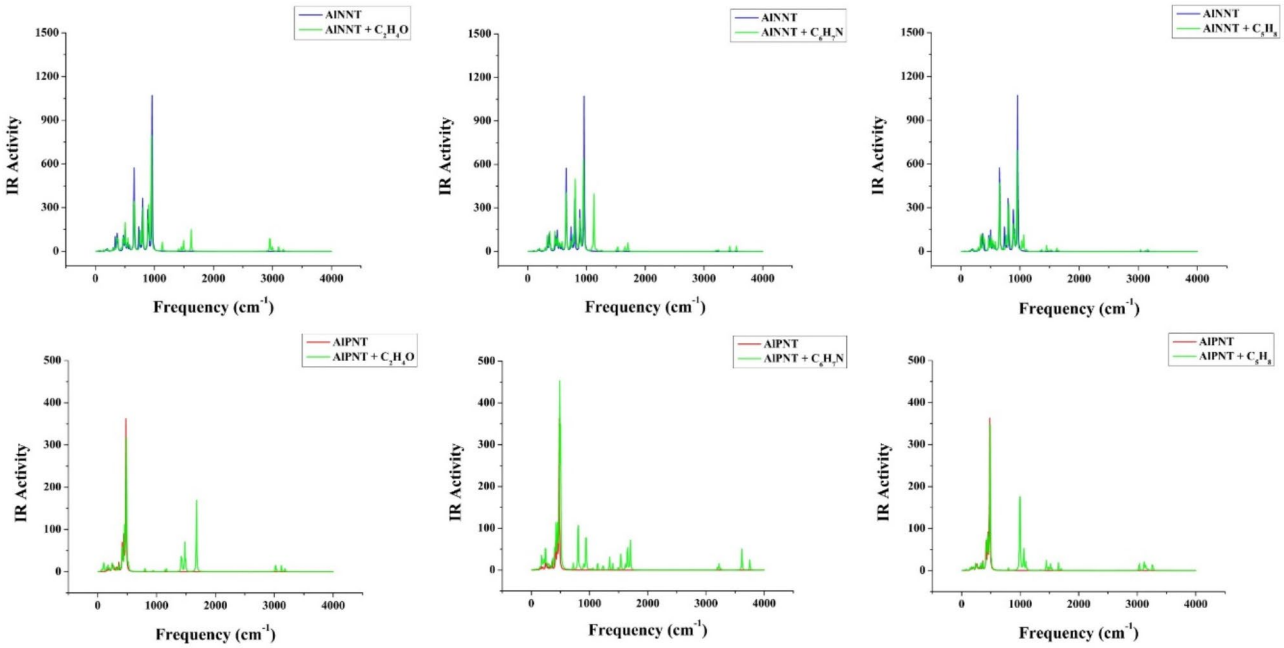

Fig. 4. The IR spectrum analysis of AlNNT and AlPNT before and after adsorbing C_2H_4O, C_6H_7N, and C_5H_8 biomarkers.

adsorbing these biomarkers on the AlNNT and AlPNT, the Mulliken charges have been redistributed because of wide ranges of electronegativity differences of the constituent atoms of adsorbent nanotubes and targeted VOCs and observed as 1.524, 1.468, 1.484, 0.686, 0.704, and 0.773e respectively for AlNNT + C_2H_4O, AlNNT + C_6H_7N, AlNNT + C_5H_8, AlPNT + C_2H_4O, AlPNT + C_6H_7N, and AlPNT + C_5H_8 complexes. This charge redistribution because of the Mulliken charge transfer from biomarkers to nanotubes confirms the electrochemical reaction between the nanotubes and biomarkers that will help to develop sensory devices with the help of AlNNT and AlPNT to detect C_2H_4O, C_6H_7N, and C_5H_8 by observing detectable electrochemical signals in the presence of these VOCs[52,60].

Natural bond orbital (NBO) analysis is very crucial for understanding the accurate transfer along with the inter or intramolecular bonding interaction of a molecular system[61]. In this work, before and after the interaction of biomarkers with studied nanotubes, the NBO charge distribution is computed and tabulated in (Table 1). The NBO charges of AlNNT and AlPNT are 2.051e and 1.137e respectively where all the group III elements (Al atoms) act as donors and all group V elements (N and P atoms) act as receivers due to their differences in electronegativities as discussed in Mulliken charge distribution section. However, during the adsorption process, some charges from C_2H_4O, C_6H_7N, and C_5H_8 biomarkers are transferred to the nanotubes and during this process, all nanotubes act as charge receivers and biomarkers are as electron donors, and the NBO charges of the complexes negatively enhanced which confirms the intermolecular interaction during the physisorption process[61,62]. So, the redistributed NBO charges after the physisorption process are 2.062, 2.076, 2.093, 1.190, 1.219, and 1.187 e respectively for AlNNT + C_2H_4O, AlNNT + C_6H_7N, AlNNT + C_5H_8, AlPNT + C_2H_4O, AlPNT + C_6H_7N, and AlPNT + C_5H_8 complexes.

In order to understand the electric property, the dipole moment is another important factor that signifies the polarity that evolves due to the asymmetric charge distribution of the constituent atoms of the molecules and a higher degree of dipole moment refers to greater electric reactivity as well as lower electric stability and vice versa[51,63]. When the dipole moment increases, higher charge asymmetry occurs which leads to the attraction of more random electrons and thus makes structures triggered to the physio absorption process[52]. The dipole moments of all structures have been measured and tabulated in (Table 2). These data reveal that, before adsorption has taken place, the dipole moments of both nanotubes are 0 Debye which means these AlNNT and AlPNT exhibit the highest electrical stability and no reactivity and the dipole moments of three biomarkers are 3.279, 1.908, and 0.754 Debye respectively for C_2H_4O, C_6H_7N, and C_5H_8. But after the adsorption process, the dipole moments of the complex system drastically improved and become 5.612, 7.803, 5.530, 4.743, 7.040, and 1.575 Debye respectively for AlNNT + C_2H_4O, AlNNT + C_6H_7N, AlNNT + C_5H_8, AlPNT + C_2H_4O, AlPNT + C_6H_7N, and AlPNT + C_5H_8 complexes. However, because of a higher degree of dipole moment for the same biomarkers, AlNNT exhibits greater reactivity than AlPNT.

Molecular orbital analyses

To understand the electric nature of the molecule, the highest occupied molecular orbital (HOMO), lowest unoccupied molecular orbital (LUMO), their gap, and Fermi energy level are some crucial factors to analyze. These factors have been measured with corresponding equations discussed in the computational description

section and tabulated in (Table 1). HOMO energy level has a direct relation with the electrical reactivity of any system and greater negative values in HOMO energy signify a higher degree of reactivity and vice versa[64]. The tabulated data reveal the HOMO energies of two nanotubes, AlNNT, and AlPNT as well as three studied biomarkers C_2H_4O, C_6H_7N, and C_5H_8 that are −5.901, −6.396, −7.143, −5.334, and −6.293 eV respectively. After adsorption of C_2H_4O, C_6H_7N, and C_5H_8 on AlNNT and AlPNT, the HOMO energies become −5.561, −5.341, −5.473, −6.179, −5.979 eV, and −6.329 respectively for AlNNT + C_2H_4O, AlNNT + C_6H_7N, AlNNT + C_5H_8, AlPNT + C_2H_4O, AlPNT + C_6H_7N, and AlPNT + C_5H_8 complexes which refers to the lower reactivity of the corresponding nanotube has observed when these biomarkers are adsorbed. Again, before adsorption, the HOMO-LUMO energy gaps of pristine AlNNT and AlPNT are 2.516 and 2.144 eV respectively but when C_2H_4O, C_6H_7N, and C_5H_8 on AlNNT and AlPNT, the energy gaps become 2.521, 2.555, 2.257, 2.166, 2.165, and 2.134 eV respectively. The energy gaps of the complex systems increase when acetaldehyde (C_2H_4O) and aniline (C_6H_7N) are adsorbed on both nanotubes but decrease when isoprene (C_5H_8) is adsorbed. This increment in the energy gap signifies the decrement of the conducting nature of the complexes and vice versa[29] which means adsorbing acetaldehyde (C_2H_4O) and aniline (C_6H_7N) causes the developing insulating nature of AlNNT and AlPNT and isoprene (C_5H_8) causes a developing conducting nature. The comparative graphical illustration of the energy gaps for the complex systems has been depicted in (Fig. 5) for a better view.

Fermi energy level is the energy of the highest occupied electrons at the absolute zero temperature which plays an important role in understanding the electronic nature and indicates the reaction process of any system[53]. The computed Fermi level is tabulated in Table 1 which shows that the Fermi energy level of pristine AlNNT and AlPNT is −4.643 and −5.324 eV respectively. When C_2H_4O, C_6H_7N, and C_5H_8 have been adsorbed in AlNNT, the Fermi energy level has been reduced and obtained −4.301, −4.063, and −4.344 eV respectively for the corresponding complexes. This reduction of Fermi energy level signifies stronger interaction between the adsorbent AlNNT and C_2H_4O, C_6H_7N, and C_5H_8 since the decrement in the forbidden gap width helps electrons to jump quickly to the conduction band as the density of states near the Fermi level increases. A similar pattern has been observed for AlPNT when C_2H_4O, C_6H_7N, and C_5H_8 have been adsorbed and these

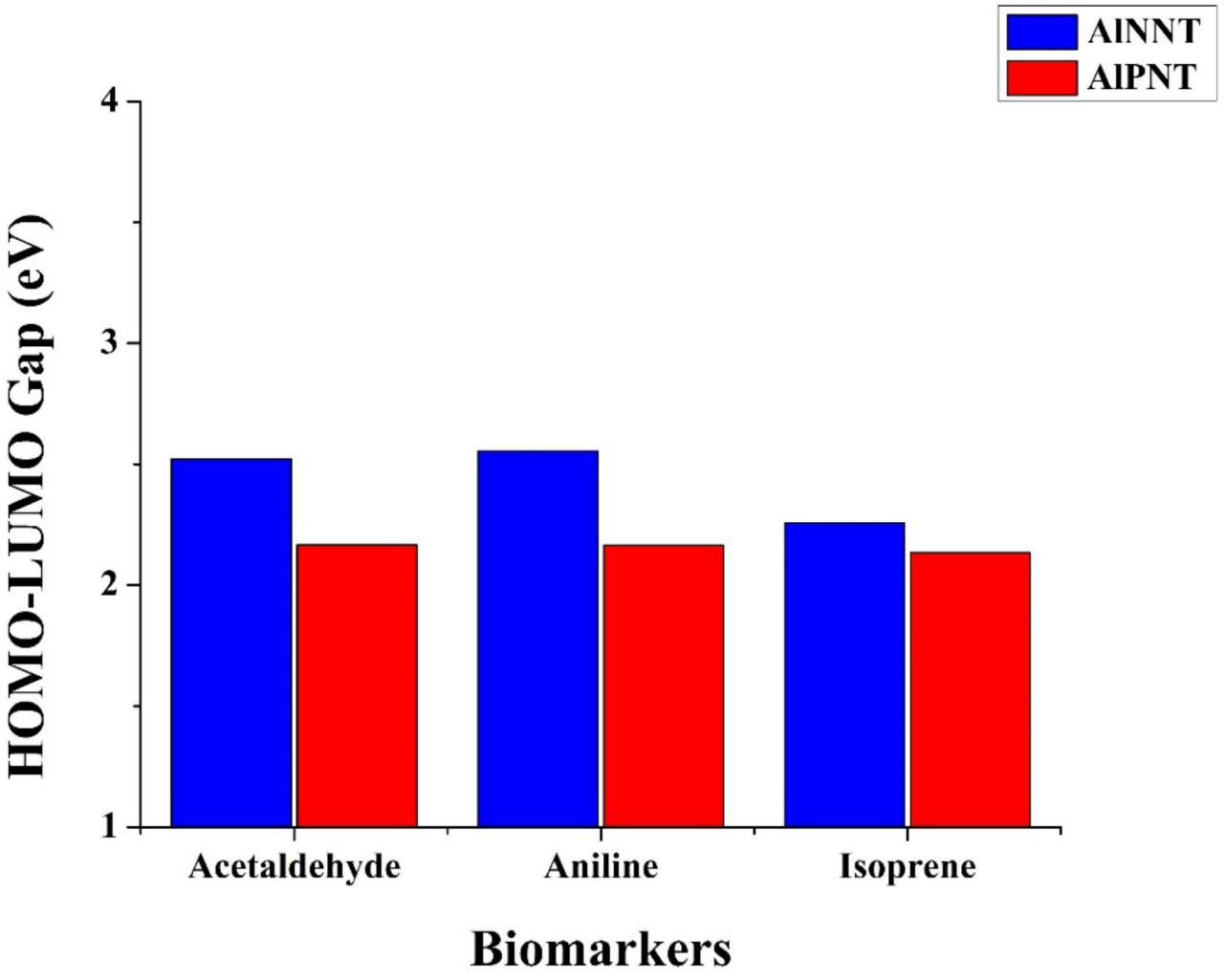

Fig. 5. Graphical presentation of the comparative HOMO-LUMO energy gaps while C_2H_4O, C_6H_7N, and C_5H_8 biomarkers have been adsorbed on AlNNT and AlPNT.

values are −5.097, −4.897 eV, and − 5.262 respectively for AlPNT + C_2H_4O, AlPNT + C_6H_7N, and AlPNT + C_5H_8 complexes. Therefore, the Fermi energy level reveals that comparing these two nanotubes, AlNNT exhibits a stronger reaction towards C_2H_4O, C_6H_7N, and C_5H_8 than AlPNT.

Density of state analysis

To understand the band gap, fluctuation of the Fermi level, and the electric behavior of any molecular system, DOS spectrum analysis is very important as it interprets the electric properties through electron density[47]. Before and after adsorbing the studied biomarkers, the DOS spectrum of AlNNT and AlPNT has been illustrated and depicted in (Fig. 6). From Fig. 6, it has been observed that, after adsorbing C_2H_4O, C_6H_7N, and C_5H_8 on both AlNNT and AlPNT, the DOS spectrum shifted to the right or the Fermi level (marked as Part I section) which refers to a stronger interaction with targeted biomarkers and adsorbent nanotubes[24]. Also, comparing the complex system for the same biomarker, AlNNT complexes exhibit greater shifting towards the Fermi level than AlPNT complexes (marked as Part II section) which supports the former finding of stronger interaction of C_2H_4O, C_6H_7N, and C_5H_8 on AlNNT than AlPNT discussed on the Fermi energy level discussion as more electrons can jump to the conduction band level and take part in interactions because of lowering width of the Fermi level.

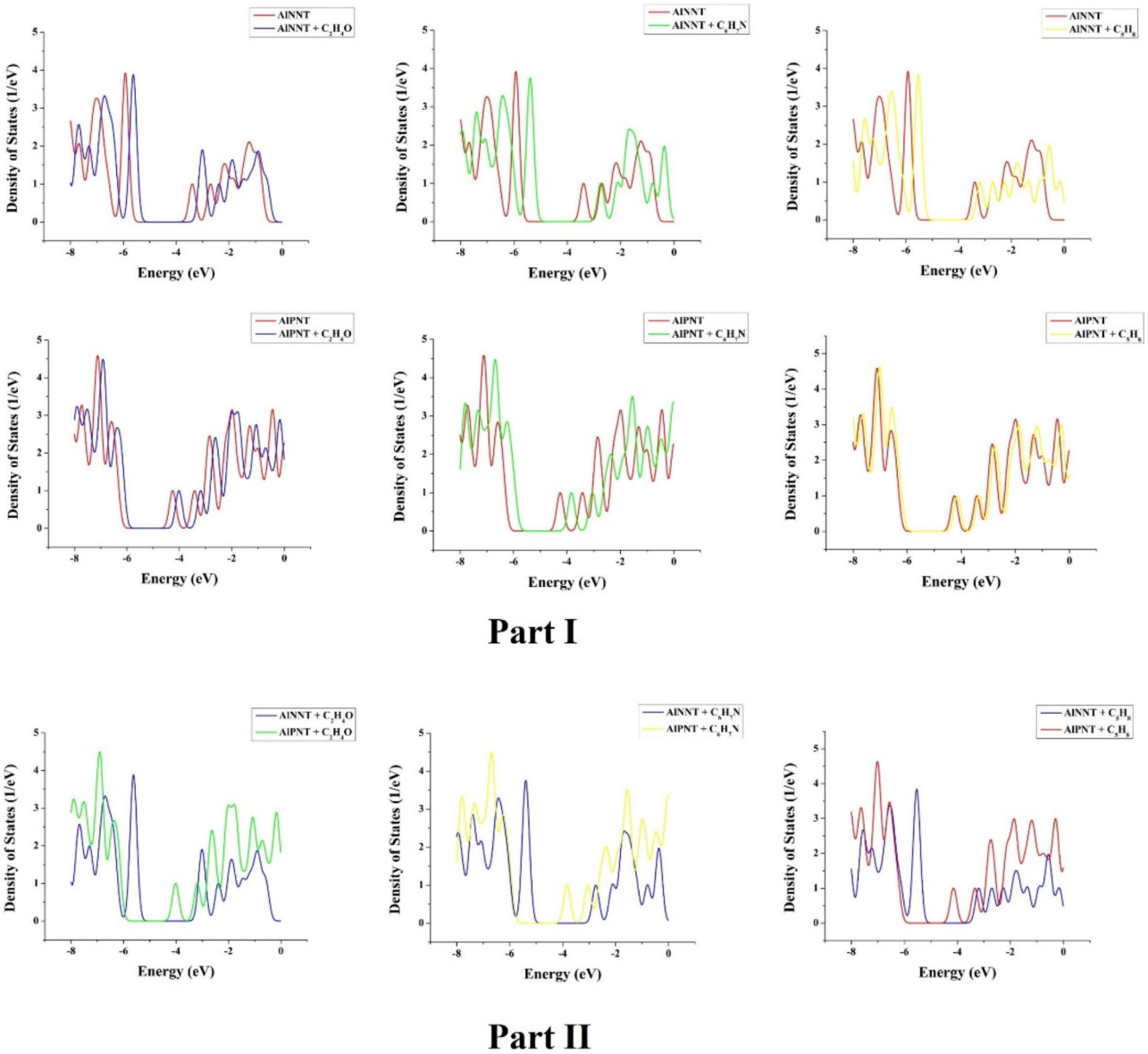

Fig. 6. The DOS spectrum of AlNNT and AlPNT before and after adsorbing C_2H_4O, C_6H_7N, and C_5H_8 biomarkers.

Thermodynamical properties analyses

To understand the thermodynamic stability of the nanotubes before and after the adsorption of the biomarkers, different thermodynamic properties changes have been measured using Eqs. (6)–(8) as discussed in the computational description section and tabulated in (Table 2). The investigation of these thermodynamic properties is very crucial because favorable optimum thermodynamic properties can help to overcome the thermodynamic desolvation penalties[65]. In this work, all the thermodynamic properties have been measured at standard room temperature to understand the viability of the reaction of the targeted biomarkers on AlNNT and AlPNT.

Changes in Gibbs free energies

Gibbs free energy is a crucial factor in order to comprehend the thermodynamic state of any reversible system which signifies the amount of reversible work at a constant temperature and pressure. Moreover, if the value of Gibbs free energy is zero, it represents the equilibrium state whereas the negative value expresses the spontaneity of states and the positive value indicates the nonspontaneous nature of the system[51,66]. The changes in the Gibbs free energy of pristine AlNNT and AlPNT are −91.86 and −60.08 eV respectively. When the lung cancer biomarkers C_2H_4O, C_6H_7N, and C_5H_8 are adsorbed on AlNNT and AlPNT, the changes in Gibbs free energies become −1.930, −2.494, −1.800, −1.421, −1.860, and −1.366 eV respectively for AlNNT + C_2H_4O, AlNNT + C_6H_7N, AlNNT + C_5H_8, AlPNT + C_2H_4O, AlPNT + C_6H_7N, and AlPNT + C_5H_8 complexes. So, it is clear that the adsorption of these biomarkers causes directing the reaction to the thermodynamic equilibrium state and for the same volatile organic compounds, adsorption in AlNNT causes more spontaneity than AlPNT. For a better understanding of the comparative Gibbs free energies of the complexes, a graphical illustration has been provided in (Fig. 7).

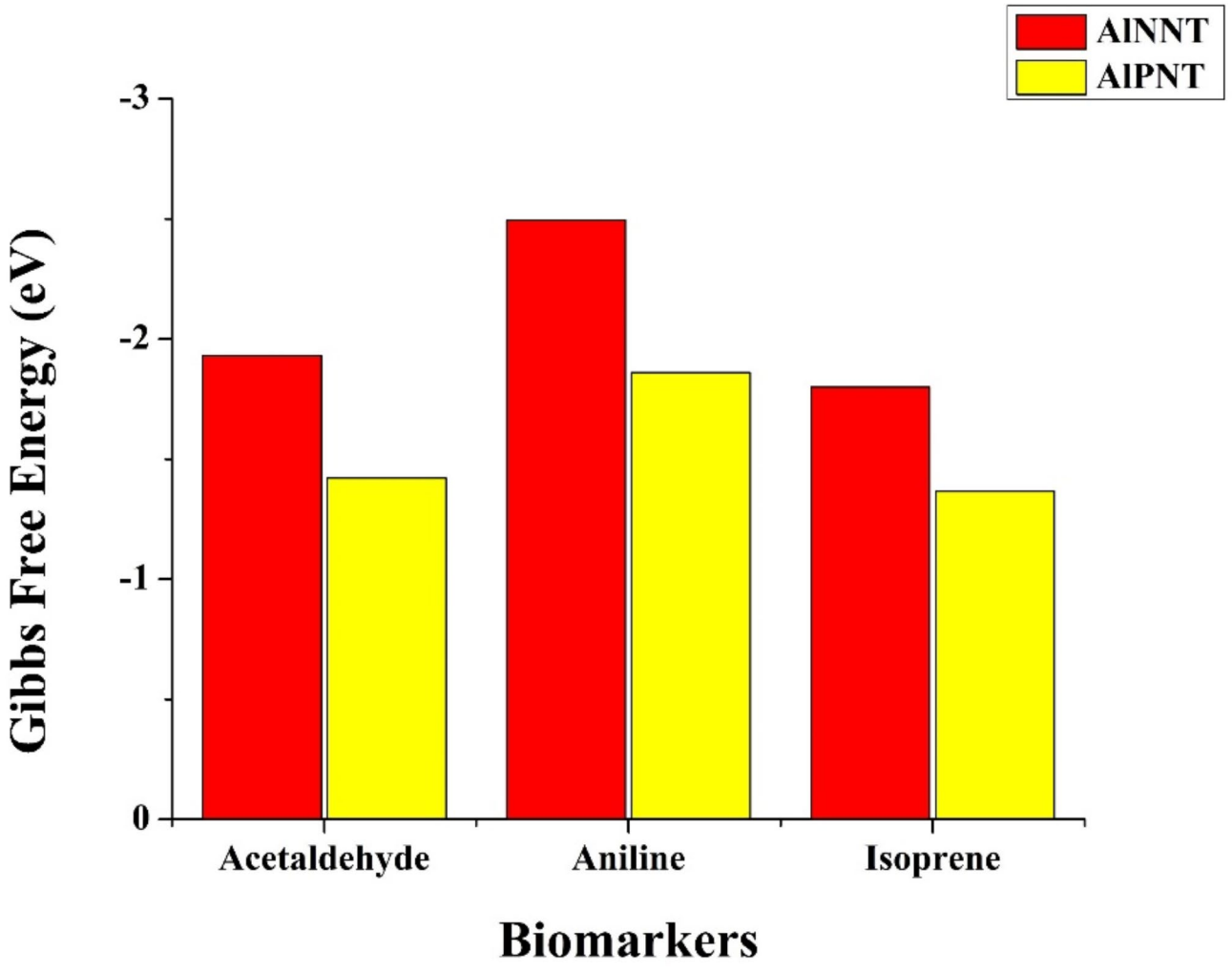

Fig. 7. Graphical illustration of the comparative analysis of the Gibbs free energy after adsorbing C_2H_4O, C_6H_7N, and C_5H_8 biomarkers on AlNNT and AlPNT.

Changes in enthalpy

The enthalpy changes refer to the nature of the system whether the reaction is endothermic or exothermic. If the value of enthalpy is positive then it refers to the endothermic nature whereas the negative values in enthalpy express the exothermic nature of the system[53]. Initially, before the adsorption process has taken place, the changes in enthalpy of AlNNT and AlPNT are −99.60 and −67.38 eV respectively. However, as C_2H_4O, C_6H_7N, and C_5H_8 are adsorbed on AlNNT and AlPNT, the changes in enthalpies become −2.458, −3.045, −2.329, −1.912, −2.43, and −1.863 eV respectively for AlNNT + C_2H_4O, AlNNT + C_6H_7N, AlNNT + C_5H_8, AlPNT + C_2H_4O, AlPNT + C_6H_7N, and AlPNT + C_5H_8 complexes. These negative values of the complex systems confirm all the structures after the adsorption process exhibit an exothermic nature and in between AlNNT and AlPNT, complexes corresponding with AlNNT will be more exothermic than AlPNT. A graphical representation has been provided to express the changes in enthalpies of the complex systems in Fig. 8 for better understanding.

Changes in entropy

To understand the orderliness of any structure, the changes in entropy signify a critical role as greater negative values in entropy refer to a higher degree of orderliness and vice versa[45]. The entropies of pristine AlNNT and AlPNT at 298.15 K are −25.94 and −24.49 meV/Mol K respectively. When the studied biomarkers have been adsorbed in these nanotubes, the orderliness decreases drastically and becomes −1.772 meV/ Mol K, −1.848 meV/ Mol K, −1.776 meV/ Mol K, −1.648 meV/ Mol K, −1.913 meV/ Mol K, and −1.666 meV/ Mol K respectively for AlNNT + C_2H_4O, AlNNT + C_6H_7N, AlNNT + C_5H_8, AlPNT + C_2H_4O, AlPNT + C_6H_7N, and AlPNT + C_5H_8 complexes. When C_2H_4O and C_5H_8 have been adsorbed into the nanotubes, AlNNT exhibits greater orderliness than AlPNT but in the case of C_6H_7N, AlPNT exhibits more orderliness than AlNNT. However, the detailed investigation of the IR frequencies revealed the increased entropy to be connected to both the vibrational and the rotational modes of the structures and this signifies an interplay between vibrational and rotational energies to further reach towards the thermodynamic equilibrium[67]. The comparative orderliness for all complexes after

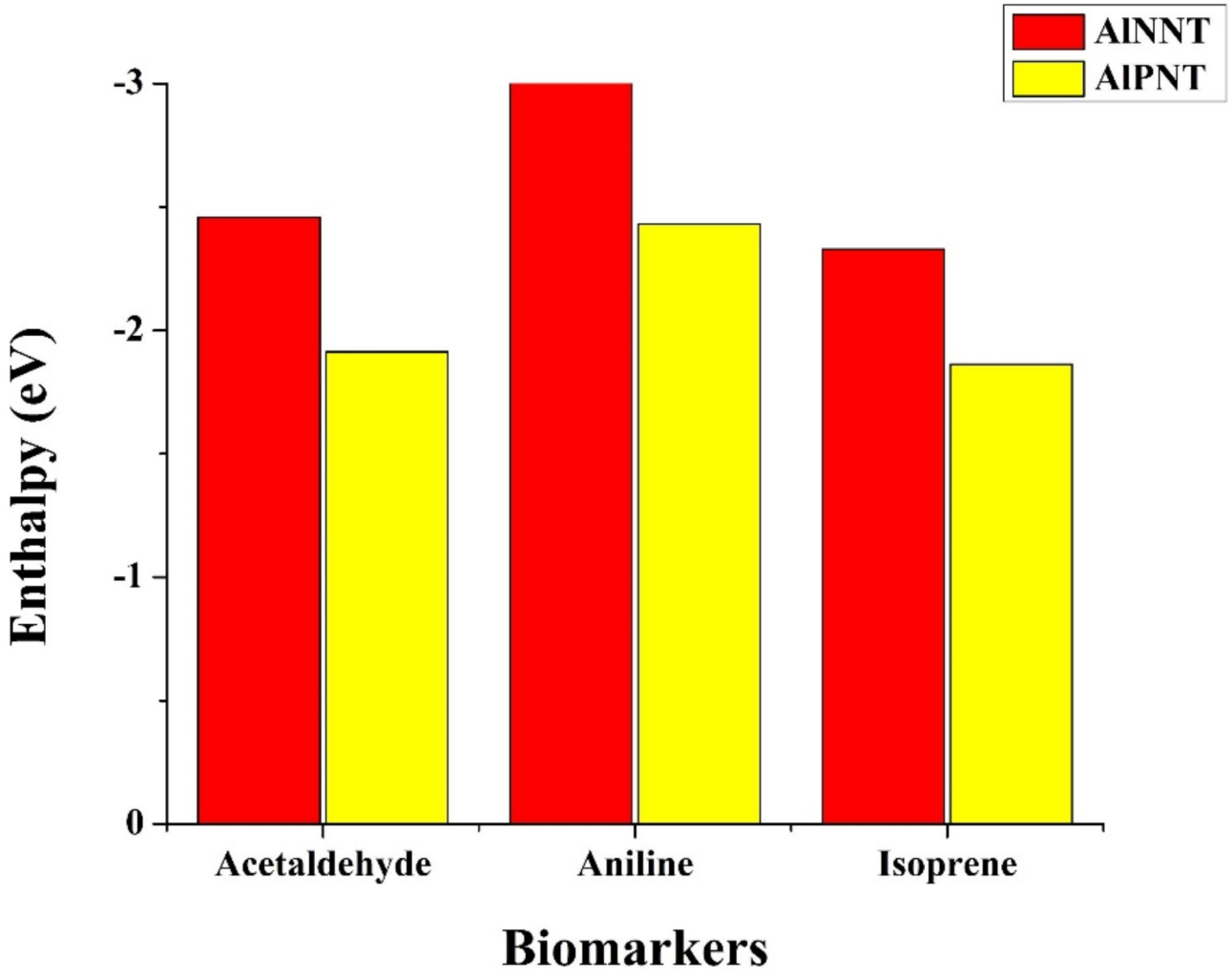

Fig. 8. Graphical representation of the comparative analysis of the enthalpies after adsorbing C_2H_4O, C_6H_7N, and C_5H_8 biomarkers on AlNNT and AlPNT.

the adsorption process has been represented graphically in order to get a better view of the changes in entropies in (Fig. 9).

Optical properties analyses

To understand the optical behavior of the AlNNT and AlPNT before and after the adsorption of C_2H_4O, C_6H_7N, and C_5H_8, the molar adsorption coefficient via ultraviolet response has been performed and visualized as UV visible spectrum. Also, the circular dichroism spectrum analyzed to understand the chirality of the systems. The initial applied frequency ranges have been taken from 300 to 1000 nm to understand the response of these structures with the corresponding complex one in this range.

UV-visible spectrum

The UV-visible spectrum gives the idea that the molecular response is in the presence of the electromagnetic spectrum[45]. In this work, the UV-visible spectrum analysis has been performed and presented in (Fig. 10). From Fig. 10, it has been observed that all the pristine and complex nanotubes exhibit molar adsorption coefficient response, and a sharp peak is observed in the range from 600 nm to 800 nm (marked in Part I). Moreover, different distinct amplitude of the complexes is the confirmation of adsorption of these biomarkers as well as suggests that the AlNNT and AlPNT can be useful in making optoelectrical sensors for detecting C_2H_4O, C_6H_7N, and C_5H_8 biomarkers and diagnosing lung cancer[52].

Circular dichroism spectrum

The circular dichroism (CD) spectrum observes when any material absorbs left and right circularly polarized light in the presence of the chiral group[45]. The CD spectrum of AlNNT and AlPNT has been illustrated before and after the adsorption process (in Fig. 10). In between pristine AlNNT and AlPNT, only AlNNT exhibits a positive CD spectrum which means pristine AlNNT absorbs circularly polarized light on the right side. When C_2H_4O, C_6H_7N, and C_5H_8 biomarkers are introduced in AlNNT, the AlNNT + C_2H_4O complex absorbs a very lower amount of circularly polarized light on the left side as CD spectrum observed in the negative Y-axis. Again,

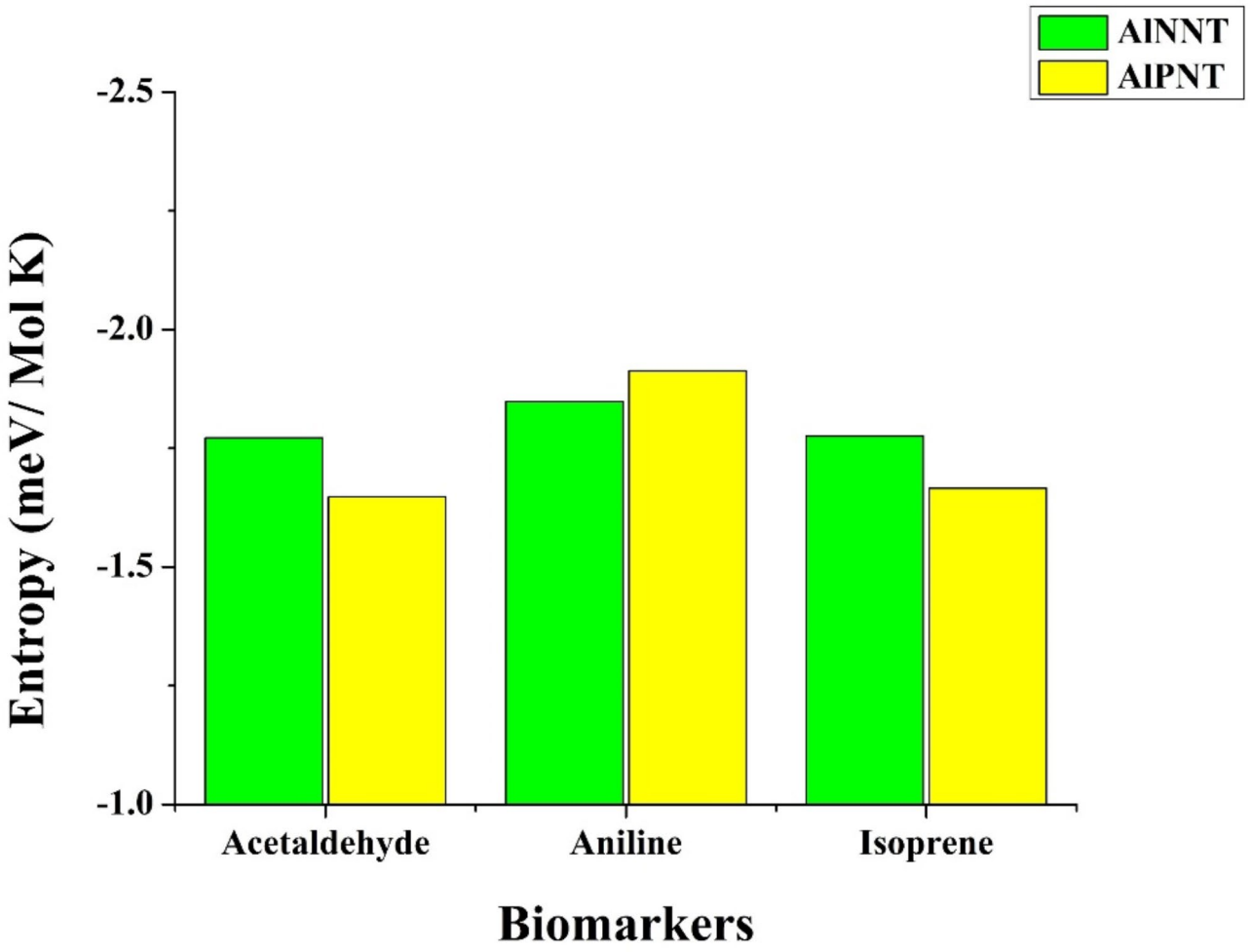

Fig. 9. A comparative graphical illustration of entropies after adsorbing C_2H_4O, C_6H_7N, and C_5H_8 biomarkers on AlNNT and AlPNT.

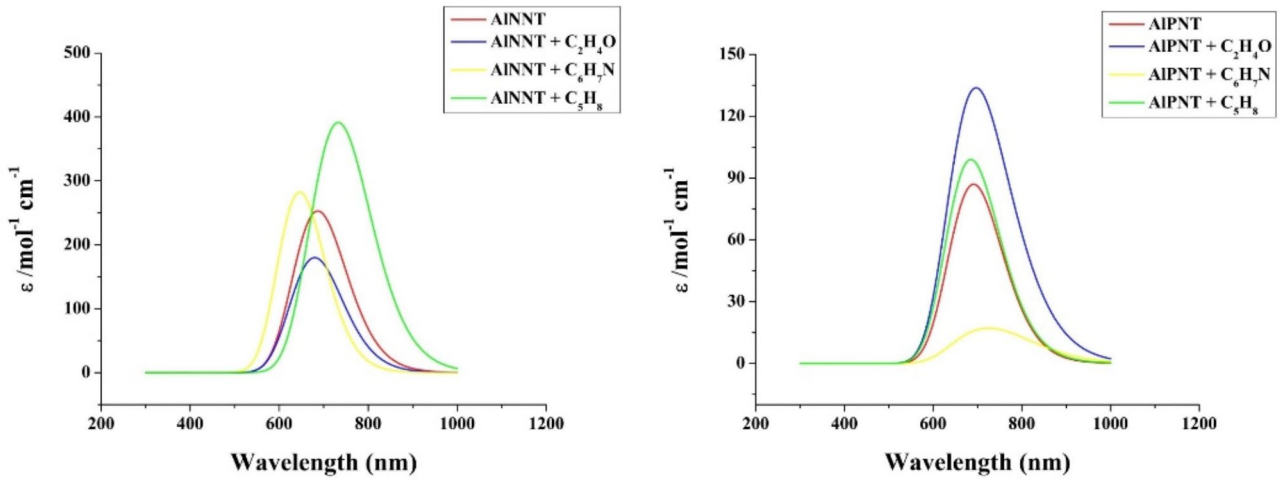

Part I: UV-Visible Spectrum

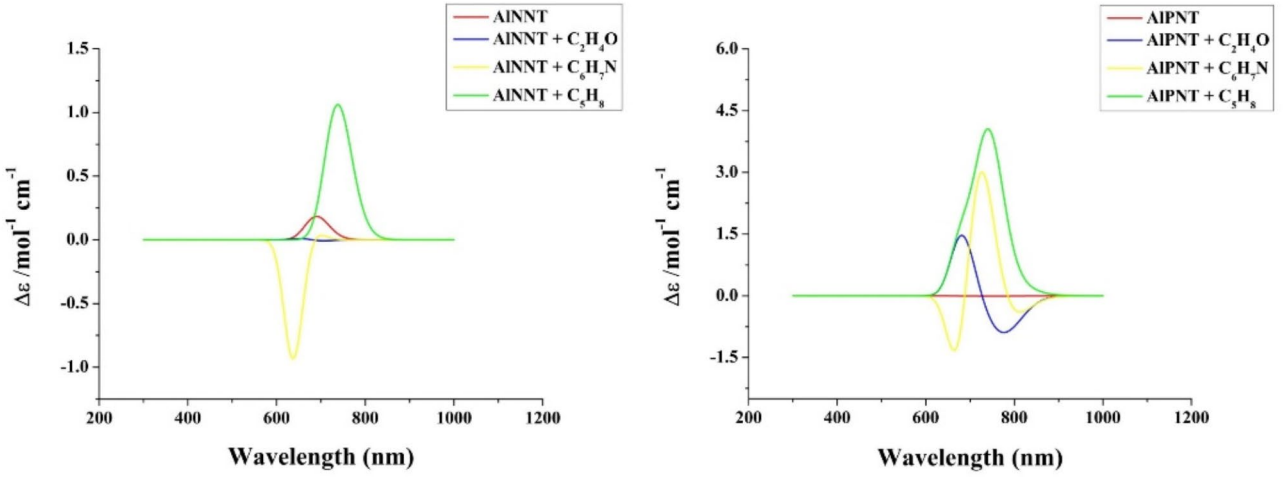

Part II: Circular Dichroism Spectrum

Fig. 10. Graphical illustration of the comparative analysis of the UV-visible spectrum and circular dichroism spectrum before and after adsorbing C_2H_4O, C_6H_7N, and C_5H_8 biomarkers on AlNNT and AlPNT.

the AlNNT + C_6H_7N complex absorbs a significant amount of circularly polarized light on the left side and the AlNNT + C_5H_8 complex absorbs a significant amount of circularly polarized light on the right side as positive Y-axis CD is observed. On the contrary, in the case of AlPNT, pristine AlPNT does not absorb any circularly polarized light as no CD spectrum is observed within the range 300 nm to 1000 nm but both the complexes that are AlPNT + C_2H_4O and AlPNT + C_6H_7N absorb circularly polarized light in both left and right direction and AlPNT + C_5H_8 absorbs circularly polarized light in right direction.

So, the UV-visible and CD spectrum analyses suggest that the adsorption of the biomarkers onto AlNNT and AlPNT nanotubes induces significant changes in their optical properties. These alterations confirm both the adsorption process and the sensitivity of these nanotubes to specific biomarkers. This sensitivity, coupled with their optical characteristics, positions AlNNT and AlPNT as promising materials for optoelectronic sensor applications for C_2H_4O, C_6H_7N, and C_5H_8. Such sensors could play a crucial role in diagnosing not only lung cancer but also any other form of cancer that may have the presence of the same biomarkers.

Conclusion

Owing to the success of gas-sensing technology, this work investigated the adsorption mechanism of three common volatile organic compound biomarkers that are acetaldehyde (C_2H_4O), aniline (C_6H_7N), and isoprene (C_5H_8) on two Aluminum-derived nanotubes- Aluminum nitride (AlN) and Aluminum phosphide (AlP) via

quantum mechanical approach DFT to understand the feasibility of these nanotubes in practical application of developing sensor to diagnose lung cancer. Therefore, different structural, electrical, thermodynamical, and optical properties analyses have been performed to understand adsorption behaviors. The adsorption energy confirms all the biomarkers will successfully adsorb on the AlNNT and AlPNT with an exothermic chemical reaction. In between AlNNT and AlPNT, AlNNT exhibits 26.30 ~ 29.66% more adsorption intensity than AlPNT for the corresponding biomarker. The adsorbing distance supports the former finding of a stronger reaction for AlNNT than AlPNT. Moreover, IR spectrum analysis reveals that the absence of imaginary frequency for both pristine and complex nanotubes is the confirmation that all the obtained optimized geometries belong to true energy minima as well as tend to form naturally. Different electrical properties such as charge analysis, molecular orbital analysis, and DOS spectrum confirm the adsorption mechanism of acetaldehyde (C_2H_4O), aniline (C_6H_7N), and isoprene (C_5H_8) on AlNNT and AlPNT. Also, the thermodynamical stability of the complex system has been examined by analyzing the changes in Gibbs free energy, enthalpy, and entropy. Considering thermodynamic stability, spontaneity, and orderliness, AlNNT is more viable than AlPNT. Also, the analysis of optical properties with the help of UV-Vis, and CD spectrum, supports the adsorption mechanism of C_2H_4O, C_6H_7N, and C_5H_8 on AlNNT and AlPNT. Therefore, considering all factors, AlNNT is more feasible to detect C_2H_4O, C_6H_7N, and C_5H_8 than AlPNT and thus has the potentiality for practical application of developing sensors to diagnose lung cancer at the preliminary stage.

Data availability

All data were used for the research described in the manuscrip.

Received: 1 November 2024; Accepted: 10 February 2025
Published online: 07 October 2025

References

1. Li, C. et al. Global burden and trends of lung cancer incidence and mortality. *Chin. Med. J.* **136** (13), 1583–1590 (2023).
2. Sharma, R. Mapping of global, regional and national incidence, mortality and mortality-to-incidence ratio of lung cancer in 2020 and 2050. *Int. J. Clin. Oncol.* **27** (4), 665–675 (2022).
3. Siddique, F., Shehata, M., Ghazal, M., Contractor, S. & El-Baz, A. Lung cancer subtyping: A short review. *Cancers* **16** (15), 2643 (2024).
4. Li, Y. et al. CircMYBL1 suppressed acquired resistance to osimertinib in non-small-cell lung cancer. *Cancer Genet.* **284**, 34–42 (2024).
5. Torre, L. A., Siegel, R. L. & Jemal, A. Lung cancer statistics. *Lung Cancer Personal. Med. Curr. Knowl. Ther.* 1–19. (2016).
6. Leiter, A., Veluswamy, R. R. & Wisnivesky, J. P. The global burden of lung cancer: current status and future trends. *Nat. Reviews Clin. Oncol.* **20** (9), 624–639 (2023).
7. Li, W. et al. Advances in the early detection of lung cancer using analysis of volatile organic compounds: from imaging to sensors. *Asian Pac. J. Cancer Prev.* **15** (11), 4377–4384 (2014).
8. Thakur, S. K., Singh, D. P. & Choudhary, J. Lung cancer identification: a review on detection and classification. *Cancer Metastas. Rev.* **39** (3), 989–998 (2020).
9. Bishara, T., Ramnani, D. M. & Epstein, J. I. High-grade prostatic intraepithelial neoplasia on needle biopsy: risk of cancer on repeat biopsy related to number of involved cores and morphologic pattern. *Am. J. Surg. Pathol.* **28** (5), 629–633 (2004).
10. Boiselle, P. M., Ernst, A. & Karp, D. D. Lung cancer detection in the 21st century: potential contributions and challenges of emerging technologies. *Am. J. Roentgenol.* **175** (5), 1215–1221 (2000).
11. Boeri, M. et al. Recent advances of microRNA-based molecular diagnostics to reduce false-positive lung cancer imaging. *Expert Rev. Mol. Diagn.* **15** (6), 801–813 (2015).
12. Nokes, B. et al. Improving the process of ordering outside genomic testing for lung cancer FNA and small biopsy specimens–A multidisciplinary quality improvement project. *Cyto J.* 20 (2023).
13. Yao, X. et al. Fusion of shallow and deep features from 18F-FDG PET/CT for predicting EGFR-sensitizing mutations in non-small cell lung cancer. *Quantitat. Imaging Med. Surg.* **14** (8), 5460. (2024).
14. Goffin, J. R. et al. Cost-effectiveness of lung cancer screening in Canada. *JAMA Oncol.* **1** (6), 807–813 (2015).
15. Ma, X. et al. Detection of breast cancer based on novel porous silicon Bragg reflector surface-enhanced Raman spectroscopy-active structure. *Chinese Opt. Lett.* **18** (5), 051701. (2020).
16. Su, Y. et al. Colon cancer diagnosis and staging classification based on machine learning and bioinformatics analysis. *Comput. Biol. Med.* **145**, 105409. (2022).
17. Tyagi, D. et al. Recent advances in two-dimensional-material-based sensing technology toward health and environmental monitoring applications. *Nanoscale* **12** (6), 3535–3559 (2020).
18. Xu, Q. et al. Recent development of multifunctional sensors based on low-dimensional materials. *Sensors* **21** (22), 7727 (2021).
19. Roberts, A., Tripathi, P. P. & Gandhi, S. Graphene nanosheets as an electric mediator for ultrafast sensing of urokinase plasminogen activator receptor—A biomarker of cancer. *Biosens. Bioelectron.* **141**, 111398 (2019).
20. Sakr, Mahmoud, A. S. et al. Theoretical investigation of quantum dot-biphenylene nanocomposites for potential nonenzymatic glucose biomarker detection using DFT simulations. *J. Alloys Compd. Commun.* 100008. (2024).
21. Cheng, H. et al. Novel ratiometric surface-enhanced Raman scattering (SERS) biosensor for ultrasensitive quantitative monitoring of human carboxylesterase-1 in hepatocellular carcinoma cells using Ag–Au nanoflowers as SERS substrate. *Anal. Chem.* **96** (46), 18555–18563 (2024).
22. de Andrade, L. R. M. et al. Biomedical applications of carbon nanotubes: a systematic review of data and clinical trials. *J. Drug Deliv. Sci. Technol.* **99**, 105932 (2024).
23. Aasi, A., Aghaei, S. M. & Panchapakesan, B. A density functional theory study on the interaction of toluene with transition metal decorated carbon nanotubes: a promising platform for early detection of lung cancer from human breath. *Nanotechnology* **31** (41), 415707. (2020).
24. Wan, Q., Zhang, X. & Gui, Y. Theoretical study on pt-doped carbon nanotubes used to detect typical exhaled gases of lung cancer. *J. Comput. Theor. Nanosci.* **12** (10), 3412–3417 (2015).
25. Chen, H. et al. Aptamer-functionalized carbon nanotube field-effect transistor biosensors for Alzheimer's disease serum biomarker detection. *ACS Sens.* **7** (7), 2075–2083 (2022).
26. Aasi, A., Aasi, E., Aghaei, S. M. & Panchapakesan, B. CNT biodevices for early liver cancer diagnosis based on biomarkers detection—A promising platform. *J. Mol. Graph. Model.* **114**, 108208. (2022).

27. Kadhim, M. M. et al. Investigating the effect of structural antisite defects on the adsorption and detection of ozone gas by AlP nanotubes. *Struct. Chem.* **34** (4), 1497–1505 (2023).
28. Kadhim, M. M. et al. The Cd-decorated AlN nanotube as a potential chemical sensor for chloropicrin: DFT studies. *Comput. Theoret. Chem.* **1220**, 113982. (2023).
29. Rahman, A. U., Saaduzzaman, D. M., Hasan, S. M. & Sikder, M. K. U. Potentiality of phosphide-based nanotubes for breast cancer detection: A DFT investigation. *Nanotechnology* **35** (36), 365701 (2024).
30. Sun, X., Shao, K. & Wang, T. Detection of volatile organic compounds (VOCs) from exhaled breath as noninvasive methods for cancer diagnosis. *Anal. Bioanal. Chem.* **408**, 2759–2780 (2016).
31. Wan, Q., Xu, Y., Chen, X. & Xiao, H. Exhaled gas detection by a novel Rh-doped CNT biosensor for prediagnosis of lung cancer: a DFT study. *Mol. Phys.* **116** (17), 2205–2212 (2018).
32. Peng, G. et al. Detection of lung, breast, colorectal, and prostate cancers from exhaled breath using a single array of nanosensors. *Br. J. Cancer* **103** (4), 542–551 (2010).
33. Nardi-Agmon, I. & Peled, N. Exhaled breath analysis for the early detection of lung cancer: recent developments and future prospects. *Lung Cancer Targ. Ther.* 31–38 (2017).
34. Tarun, T. et al. Defective GaAs nanoribbon–based biosensor for lung cancer biomarkers: a DFT study. *J. Mol. Model.* **27** (9), 270. (2021).
35. Korucu, Ş., Kose, A. & Fellah, M. F. Biosensor for the early diagnosis of lung cancer: A DFT study on the applicability of metal-doped graphene structures. *Sens. Actuat. A Phys.* **376**, 115637 (2024).
36. Wan, Q., Xu, Y. & Zhang, X. Adsorption properties of typical lung cancer breath gases on Ni-SWCNTs through density functional theory. *J. Sens.* **2017** (1), 7974545 (2017).
37. Dennington, R., Keith, T. & Millam, J. GaussView, version 6. (2009).
38. Singh, J. S., Khan, M. S. & Uddin, S. A DFT study of vibrational spectra of 5-chlorouracil with molecular structure, HOMO–LUMO, MEPs/ESPs and thermodynamic properties. *Polym. Bull.* **80** (3), 3055–3083 (2023).
39. Ismail, A. M., Ezzat, H. A., Menazea, A. A. & Ibrahim, M. A. Synthesis, molecular spectroscopic analyses, and computational investigation using DFT: B3LYP/LANL2DZ calculations for PVC/PANI/GO composite. *J. Electron. Mater.* **50** (8), 4741–4751 (2021).
40. Fiori-Duarte, A. T. et al. A new palladium (II) complex with ibuprofen: spectroscopic characterization, DFT studies, antibacterial activities and interaction with biomolecules. *J. Mol. Struct.* **1186**, 144–154 (2019).
41. De Souza, L. A., Almeida, E. R., Belchior, J. C., Santos, D. & De Almeida, H. F. W.B., Cisplatin release from inclusion complex formed by oxidized carbon nanotube: A DFT study. *Chem. Phys. Lett.* **774**, 138619 (2021).
42. Torres, E. & DiLabio, G. A. A (nearly) universally applicable method for modeling noncovalent interactions using B3LYP. *J. Phys. Chem. Lett.* **3** (13), 1738–1744 (2012).
43. Frisch, M. J. E. A. et al. Gaussian 09, Gaussian. Inc., Wallingford CT. **121**, 150–166 (2009).
44. Liang, W., Zhao, Y. & Head-Gordon, M. An efficient approach for self-consistent-field energy and energy second derivatives in the atomic-orbital basis. *J. Chem. Phys.* **123** (19). (2005).
45. Rahman, A. U. et al. A comparative DFT investigation on the structural, electric, thermodynamic, and optical properties of the pristine and various metals and nonmetals (Li, be, B, N, o, and F) doped graphene and silicene nanosheets. *Phys. B Condens. Matter* **675**, 415615 (2024).
46. Pinhal, G. B., Marana, N. L., Fabris, G. S. & Sambrano, J. R. Structural, electronic and mechanical properties of single-walled AlN and GaN nanotubes via DFT/B3LYP. *Theor. Chem. Acc.* **138**, 1–11 (2019).
47. Rahman, A. U., Saaduzzaman, D. M., Hasan, S. M. & Sikder, M. K. U. Feasibility of implanting gold-doped silicon nanoclusters (Si 8) as electrode for dopamine detection: A DFT investigation. In *2023 5th International Conference on Sustainable Technologies for Industry 5.0 (STI)* 1–5 (IEEE, 2023).
48. Ahmed, M. T., Roman, A. A., Roy, D., Islam, S. & Ahmed, F. Phosphorus-doped T-graphene nanocapsule toward O3 and SO2 gas sensing: a DFT and QTAIM analysis. *Sci. Rep.* **14** (1), 3467 (2024).
49. Srivastava, R., Suman, H., Shrivastava, S. & Srivastava, A. DFT analysis of pristine and functionalized zigzag CNT: A case of H2S sensing. *Chem. Phys. Lett.* **731** 136575. (2019).
50. Muktadir, M. G., Alam, A., Piya, A. A. & Shamim, S. U. D. Exploring the adsorption ability with sensitivity and reactivity of C 12–B 6 N 6, C 12–Al 6 N 6, and B 6 N 6–Al 6 N 6 heteronanocages towards the cisplatin drug: a DFT, AIM, and COSMO analysis. *RSC Adv.* **12** (45), 29569–29584 (2022).
51. Rahman, A. U., Saaduzzaman, D. M., Hasan, S. M. & Sikder, M. K. U. A DFT study of structural, electrical, and thermodynamical properties of sc, Ti, V doped ring beryllium oxide (BeO) n (n = 3–5) nanoclusters. *AIP Adv.* **14** (5). (2024).
52. Rahman, H., Hossain, M. R. & Ferdous, T. The recent advancement of low-dimensional nanostructured materials for drug delivery and drug sensing application: A brief review. *J. Mol. Liquids* **320** 114427. (2020).
53. Hossain, M. R. et al. First-principles study of the adsorption of chlormethine anticancer drug on C24, B12N12 and B12C6N6 nanocages. *Computat. Theoret. Chem.* **1197**, 113156 (2021).
54. Khan, M. I. et al. Exploring the sensing potential of Fe-decorated h-BN toward harmful gases: a DFT study. *RSC Adv.* **14** (10), 7040–7051 (2024).
55. Liu, H. et al. The adsorption and sensing performances of Ir-modified MoS2 monolayer toward SF6 decomposition products: a DFT study. *Nanomaterials* **11** (1), 100 (2021).
56. Cal, M. P., Strickler, B. W., Lizzio, A. A. & Gangwal, S. K. High temperature hydrogen sulfide adsorption on activated carbon: II. Effects of gas temperature, gas pressure and sorbent regeneration. *Carbon* **38** (13), 1767–1774 (2000).
57. Fouad, R., Shaaban, I. A., Ali, T. E., Assiri, M. A. & Shenouda, S. S. Co (II), ni (II), Cu (II) and cd (II)-thiocarbonohydrazone complexes: spectroscopic, DFT, thermal, and electrical conductivity studies. *RSC Adv.* **11** (60), 37726–37743 (2021).
58. Franco-Pérez, M. & Gázquez, J. L. Electronegativities of pauling and mulliken in density functional theory. *J. Phys. Chem. A* **123** (46), 10065–10071 (2019).
59. Pauling, L. *The Nature of the Chemical bond and the Structure of Molecules and Crystals: An Introduction to Modern Structural Chemistry* 18 (Cornell University Press, 1960).
60. Das, A. et al. Adsorption behavior of hydrogen selenide gas on the surfaces of pristine and Ni-doped X12Y12 (X = Al, B and Y = N, P) nano-cages: a first-principles study. *Struct. Chem.* **34** (4), 1439–1456 (2023).
61. Rahuman, M. H., Muthu, S., Raajaraman, B. R., Raja, M. & Umamahesvari, H. Investigations on 2-(4-Cyanophenylamino) acetic acid by FT-IR, FT-Raman, NMR and UV-Vis spectroscopy, DFT (NBO, HOMO-LUMO, MEP and Fukui function) and molecular docking studies. *Heliyon* **6** (9). (2020).
62. Hassani, N. & Mehdizade, M. Exploring the adsorption and sensing behavior of the M-Nx-B36-x (M = Fe, Ni, and Cu; x = 0, 3) bowl-shaped structures upon CO, NO, O_2, and N_2 molecules: a first-principles study. *Phys. E Low Dimens. Syst. Nanostruct.* **124**, 114242 (2020).
63. Daswani, U., Singh, U., Sharma, P. & Kumar, A. From molecules to devices: a DFT/TD-DFT study of dipole moment and internal reorganization energies in optoelectronically active aryl azo chromophores. *J. Phys. Chem. C* **122** (26), 14390–14401 (2018).
64. Ahmed, M. T., Islam, S. & Ahmed, F. Structural, optical, and electronic properties of boron nitride incorporated mobius carbon nanoribbon: a DFT calculation. *Phys. Scripta* **98** (3), 035827. (2023).
65. Gholizadeh, S. et al. Mode of binding, kinetic and thermodynamic properties of a lipid-like drug (Fingolimod) interacting with Human Serum Albumin. *BioImpacts BI* 13 (2), 109. (2022).

66. Sozbilir, M. Turkish chemistry undergraduate students' misunderstandings of Gibbs free energy. *Univ. Chem. Educ.* **6** (2), 73–83 (2002).
67. Vranken, I., Baudry, J., Aubinet, M., Visser, M. & Bogaert, J. A review on the use of entropy in landscape ecology: heterogeneity, unpredictability, scale dependence and their links with thermodynamics. *Landsc. Ecol.* **30**, 51–65 (2015).

Acknowledgements
The authors are thankful to the Biophysics Lab, Dept. of Physics, Jahangirnagar University for providing us with the computational resources for this work.

Author contributions
Aoly Ur Rahman: Conceptualization, Data curation, Formal analysis, Investigation, Methodology, Writing—original draft, Writing—review & editing. D.M. Saaduzzaman: Writing—review & editing. Syed Mahedi Hasan: Writing—review & editing. Muzzakkir Amin: Writing—review & editing. Md. Kabir Uddin Sikder: Resource, Supervision.

Declarations

Competing interests
The authors declare no competing interests.

Additional information
Correspondence and requests for materials should be addressed to A.U.R.

Reprints and permissions information is available at www.nature.com/reprints.

Publisher's note Springer Nature remains neutral with regard to jurisdictional claims in published maps and institutional affiliations.

Open Access This article is licensed under a Creative Commons Attribution-NonCommercial-NoDerivatives 4.0 International License, which permits any non-commercial use, sharing, distribution and reproduction in any medium or format, as long as you give appropriate credit to the original author(s) and the source, provide a link to the Creative Commons licence, and indicate if you modified the licensed material. You do not have permission under this licence to share adapted material derived from this article or parts of it. The images or other third party material in this article are included in the article's Creative Commons licence, unless indicated otherwise in a credit line to the material. If material is not included in the article's Creative Commons licence and your intended use is not permitted by statutory regulation or exceeds the permitted use, you will need to obtain permission directly from the copyright holder. To view a copy of this licence, visit http://creativecommons.org/licenses/by-nc-nd/4.0/.

© The Author(s) 2025